Sensors and Actuators A 263 (2017) 198–208

Contents lists available at ScienceDirect

Sensors and Actuators A: Physical

journal homepage: www.elsevier.com/locate/sna

Non-invasive vascular resistance monitoring with a piezoelectric sensor and photoplethysmogram

Lu Wang [a], Sardar Ansari [b], Daniel Slavin [a], Kevin Ward [b], Kayvan Najarian [c], Kenn R. Oldham [a,*]

[a] Department of Mechanical Engineering, University of Michigan, G.G. Brown Laboratory, 2650 Hayward St., Ann Arbor, MI 48109 USA
[b] Department of Emergency Medicine, University of Michigan, Building 10-103A, North Campus Research Complex, Ann Arbor, MI 48109 USA
[c] Department of Computational Medicine and Bioinformatics, Department of Emergency Medicine, and Department of Electrical Engineering and Computer Science, University of Michigan, Building 10-103A, North Campus Research Complex, Ann Arbor, MI 48109 USA

ARTICLE INFO

Article history:
Received 18 October 2016
Received in revised form 15 May 2017
Accepted 5 June 2017
Available online 20 June 2017

Keywords:
Piezoelectric sensing
Photoplethysmogram
Cardiovascular monitoring
Vascular resistance
Modeling

ABSTRACT

Peripheral vascular resistance is known to be a key indicator of the body's efforts to compensate for cardiovascular stresses, but remains very difficult to assess with existing technology. In this work, changes in vascular tone are estimated non-invasively by observing variation in response of a photoplethysmogram and a novel piezoelectric cardiovascular sensor. A simple model of the piezoelectric sensor and underlying artery and tissue is derived to capture trends in relative amplitude and hysteresis between the two sensors, and metrics for estimating vascular resistance based on these trends are proposed. Vascular resistance tracking results are demonstrated to show strong correlation with invasively-measured systemic vascular resistance in swine subjects.

1. Introduction

The state of the peripheral arteries is known to be a key physiological indicator of the body's response to both acute and chronic medical conditions. For example, the body's vascular tone, or constriction of the arteries relative to a maximally dilated state, is a direct indicator of the body's response to cardiovascular stress. Peripheral arterial constriction or dilation is also the dominant factor in determining the body's systemic vascular resistance (SVR), or resistance felt by the heart in forcing blood through the circulatory system; SVR is a major means of compensation to maintain physiological homeostasis. Situations where rapid changes in vascular tone and SVR are known to have great importance include shock (sepsis, cardiac, traumatic, etc.) [1–3], post-surgical recovery [4,5], and dialysis [6].

Despite the potential value of being able to monitor vascular tone and SVR continuously and rapidly, existing technology for acquiring this information is severely limited. This is especially true of continuous, non-invasive technologies. Peripheral artery diameter can be directly measured only through biomedical imaging, typically ultrasound [7,8]; acoustic techniques have also been proposed for measuring SVR [9]. However, imaging is not available on a continuous basis or in most care settings. The gold standard for SVR measurement is invasive monitoring of cardiac output, central venous pressure, and arterial pressure through catheterization. However, this is available only in intensive care settings, and not universally even then. Researchers have also proposed improvements on vascular resistance measurements by applying more complex models to aortic flow data [10,11]. Non-invasive systems for estimating cardiac output, and from there inferring SVR, have been commercialized based on electrical cardiometry [12] and whole body bioimpedance [13]. However, these track SVR only weakly [14,15], since central venous pressure is not measured, and are also unavailable outside of acute medical care settings.

Researchers have thus pursued methods for estimating SVR and vascular tone using simpler instruments. Prior attempts have generally relied on photoplethysmogram (PPG) data, which tracks changes in artery volume within short-term pulse cycles. Timing of reflection waves as extracted from PPG data has been reported to indicate changes in peripheral arterial resistance, but this was only

* Corresponding author.
E-mail addresses: wangluhy@umich.edu (L. Wang), sardara@umich.edu (S. Ansari), keward@umich.edu (K. Ward), kayvan@umich.edu (K. Najarian), oldham@umich.edu (K.R. Oldham).

http://dx.doi.org/10.1016/j.sna.2017.06.007
0924-4247/

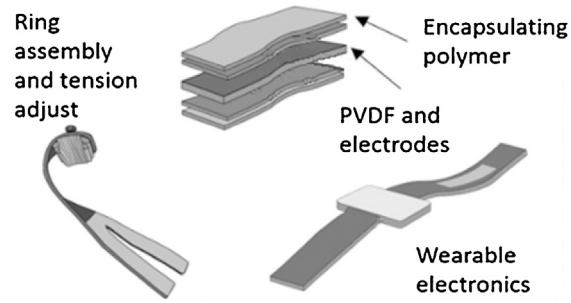

Fig. 1. Compliant polyvinylidene fluoride (PVDF) piezoelectric sensing band for non-invasive artery monitoring.

verified through basic correlations with expected trends among hypertension subjects, not individualized tracking [16]. Methods for extracting SVR from multiple regression of PPG waveform data points have been derived by machine learning techniques, but SVR estimation error ranged from 15%–100% for most subjects [17,18]. Evaluating a vascular tone index by matching models for arterial dynamics to pulse transit time (PTT) and blood pressure (BP) measurements has also been proposed [19]. However, results could at most be correlated with risk factors for high SVR, rather than SVR itself. Another report showed PTT correlation with SVR over time, but only for two individual cases [20]. Estimates of cardiac output and vascular resistance have also been suggested based on ECG and BP cuff data, and used in tracking response to physical activity, but these are recognized as only approximate measures [21].

This paper proposes a technique for tracking changes in vascular tone by combining PPG data with measurements from an adjacent compliant piezoelectric polymer pressure sensor (polyvinylidene fluoride, or PVDF). Non-invasive piezoelectric arterial pressure sensing with sensors fabricated from PVDF films were likewise previously used for waveform monitoring at the human wrist by Sur et al. [22] for pulse and respiration monitoring at the chest by Chiu et al. [23] Even smaller sensing elements have been proposed based on thin-film lead-zirconate-titanate (PZT) in a polymer film [24], nanowire-impregnated polymers [25], and amorphous PZT films [26]. Regardless of transduction method, this work examines the importance of a compliant sensing structure to contrast to existing PPG measurements to track changes in vascular resistance.

In this work, a model is derived to account for the most prominent features of interaction between underlying tissue and a compliant piezoelectric sensor. A simple local model for viscoelastic dynamic behavior of the underlying artery and surrounding tissue is generated and coupled to the piezoelectric sensor model, from which variations in relative amplitude and hysteresis between the piezoelectric and PPG signals are found to show strong correlations with invasively measured SVR data in animal subjects (swine).

2. Sensor description

The authors use a custom-built flexible piezoelectric sensor for acquiring pressure signals during vascular resistance tracking, as well as an off-the-shelf PPG sensor (OXY200 and BioNomadix, BIOPAC Systems Inc.). The piezoelectric sensor may be applied to a variety of sites on the body, such as the wrist, elbow, or ankle. For vascular tone monitoring experiments on it is worn on a finger for human subjects, adjacent to a finger having a PPG sensor, and on the foreleg for swine (analogous to the human wrist), again adjacent to a PPG sensor. It is important to note that given placement of the sensor, estimated changes in vascular resistance obtained from the sensor are strictly speaking based on changes in vascular resistance of the peripheral arteries, which may in some circumstances differ from other contributing factors to SVR. Nonetheless, changes in peripheral vascular resistance and SVR are anticipated to be highly correlated, and in this work validation data available from swine testing was from SVR and indeed was seen to track closely with changes in PVDF and PPG sensor behavior.

The piezoelectric sensor, shown in Fig. 1, consists of a polymer laminate with a piezoelectric PVDF sensing layer (52 μm thick, silver plated, Precision Acoustics) between protective layers of polyimide tape (Kapton Tape, Uline Inc.), which is worn under a Velcro or elastic band. A set screw allows adjustment of the sensor to a relatively consistent level of tension. The sensor is shown applied to a sample swine subject in Fig. 2. Dedicated sensing circuits and a data-logging microcontroller are available, or the sensors can be connected directly to commercial biomedical data acquisition systems (e.g., DA100C, BIOPAC Systems Inc.), with the latter being used to acquire data presented in this work.

A sample time response of the piezoelectric sensor on the foreleg of a swine subject over three cardiac cycles is shown in Fig. 3a. The unprocessed response of the piezoelectric sensor can be considered as approximately the time derivative of pressure at the site, with this differentiation of the underlying piezoelectric pressure response resulting from high-pass filtering effects of internal capacitance and input impedance of the piezoelectric element, discussed further in Section 3.2. However, tissue and artery motion further mediate the signal as they interact with the compliant sensor, in addition to some electrical filtering. Thus, integration of the raw PVDF signal (Fig. 3b) returns a similar but not identical waveform to non-invasive blood pressure measurements (CNAP Monitor, CNSystems Medizintechik AG), in which feedback control holds artery volume constant, or to invasive arterial lines. PPG data from the same swine, shown in Fig. 3c, is comparatively less detailed, which has tended to impede its success in monitoring vas-

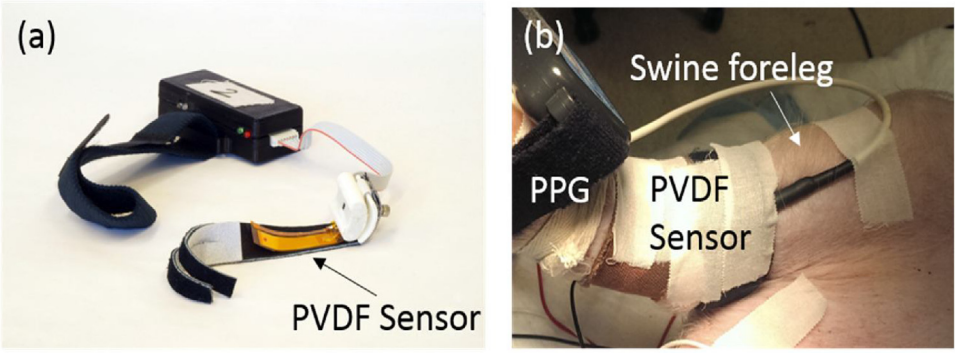

Fig. 2. (a) Example polyvinylidene fluoride (PVDF) sensor; (b) sensor applied to foreleg of swine test subject.

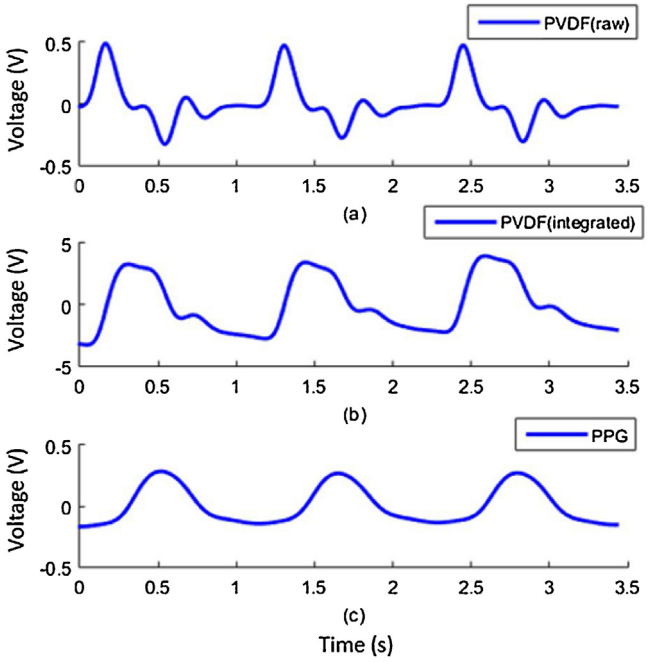

Fig. 3. Sample signals from swine subject of (a) compliant piezoelectric ring output; (b) Integrated piezo signal corresponding to fluctuations in pressure at tissue surface under ring; (c) PPG waveforms with less detail but alternate dependence on perturbations to arterial radius.

cular tone in previous studies. However, as will be discussed, the difference in dynamics between PPG and piezoelectric pressure sensor measurements as they respond to changes in the internal artery may provide important information on artery status.

3. Modeling

3.1. Photoplethysmogram (PPG)

The first sensor used in the proposed vascular resistance tracking scheme is a commercial PPG. In a PPG sensor, the change in artery volume is detected by illuminating the skin with the light from a light-emitting diode (LED) and then measuring the amount of light transmitted to a photodiode. A photodetector converts light energy into an electrical current, which connects to low noise electronic circuitry that includes a transimpedance (current-to-voltage) amplifier and filtering circuitry. A high pass filter reduces the size of the dominant DC component and enables the pulsatile AC component to be amplified. A low-pass filter is also used to remove the unwanted higher frequency noise such as electric interference (i.e. 60 Hz noise).

The voltage output of the PPG sensor is, ideally, proportional to the change of the artery's volume. However, due to the transimpedance amplification and need for high-pass filtering to obtain the time-varying component of the light signal, PPG sensors do not provide long term tracking of mean absolute arterial volume, but rather respond to short term fluctuations in arterial volume during cardiac cycles. In effect, changes in volume are convoluted with amplifier and filter dynamics, which include a differentiation, then integrated to return the relative volume fluctuations. As a model, PPG voltage output, u_{PPG}, is given by

$$u_{PPG} = K_{PPG} \int h_{PPG} * V_i dt = K_{PPG} \int h_{PPG} * \pi r_i^2 L_{PPG} dt \quad (1)$$

where K_{PPG} is the gain of the PPG sensor, h_{PPG} is the linear dynamic filter response, and V_i is volume of oxygenated blood between the

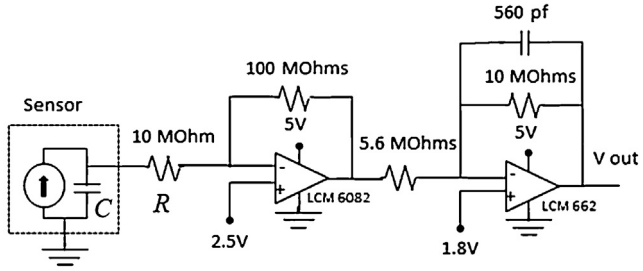

Fig. 4. Piezoelectric sensing circuit design used to model electrical dynamics of sensor interface to data acquisition system. PVDF sensor capacitance, C, and initial input resistance, R, produce a high-pass filtering effect on pressure signal, while overall gain, K_{amp}, and low-pass filtering of noise above frequency ω_{LPF} are set by remaining circuitry.

LED and photodetector, which can alternatively be related to the inner radius of the artery r_i and length of artery illuminated by the PPG, L_{PPG}. This length of the artery under PPG sensor is assumed to be constant. The exact filter in the PPG sensor is not disclosed by the manufacturer, but an approximate model used for this work was based on literature reports [27], and experimentally produced a response consistent with information from invasive sensors. This nominal PPG filter model used was

$$H_{PPG}(s) = \frac{6s}{(s+2)(s+100)} \quad (2)$$

3.2. Piezoelectric sensor: electrical

The second sensor used was the piezoelectric PVDF pressure sensing ring. In the electrical domain, the piezoelectric sensor can be modeled as a charge source in parallel with the sensor's capacitance. A high impedance charge mode amplifier, such as the BIOPAC data acquisition system used in this work, converts electrical charge to voltage. To account for interface circuit dynamics, a custom-built electrical circuit was designed that provided comparable frequency response to the BIOPAC system and the schematic of this circuit shown in Fig. 4. The sensing circuit must compensate for very low current from the PVDF sensor, measured around 1–5 nA. The nominal sensing circuit consists of a first stage amplifier, followed by a low pass filter that helps minimize electrical interference and high frequency noise.

Charge, q, generated on the PVDF sensor is given by

$$q = d_{31} E A \varepsilon_1 \quad (3)$$

where d_{31} is the piezoelectric strain coefficient from tangential strain to charge displacement in the electrode direction, E is the elastic modulus of the PVDF, A is the surface area of the PVDF, and ε_1 is the tangential strain in the PVDF layer. In this model, compressive piezoelectric response (i.e. piezoelectric strain coefficient in the axial or electrode direction, d_{33}) and coupling effects are neglected as small compared to the dominant response from hoop stress around the ring formed by the sensor.

Fig. 4 shows the combined electrical model of the PVDF sensor and sensing circuit, with resulting transfer function, $H_{PVDF}(s)$:

$$H_{PVDF}(s) = \frac{s}{RCs+1} \cdot \frac{K_{amp}\omega_{LPF}}{s+\omega_{LPF}} = \frac{18s}{(s+6)(s+178)} \quad (4)$$

where R is the input resistance to the sensing circuit (10 MOhm), C is the PVDF sensor capacitance, K_{amp} is the net amplifying circuit gain, and ω_{LPF} is a low pass filtering frequency set by the second stage of the sensing circuit.

Importantly, even with a relatively large amplifier resistance used to maintain a high input impedance for the small capacitance and charge generation of the PVDF material, the RC time constant of the sensor is small, and its associated corner frequency in (4) is

much higher than frequencies of interest in the pressure waveform. Thus, the raw voltage output of sensing circuit is approximately proportional to the derivative of the charge generated or pressure, as noted in Section 2.

In this work, variation in pressure experienced by the PVDF sensor is to be used, which is obtained by integrating the convolution of the time-varying charge with the amplifier dynamic response from (4), h_{pvdf}, to produce a the final PVDF sensor output used for analysis, u_{pvdf},

$$u_{PVDF} = \int h_{PVDF}(t) * q(t)\, dt. \tag{5}$$

Again, he integration is required because the small charge amplitude and relative impedance of the sensor result in a high-pass filter cut-off frequency much higher than the frequency of cardiac cycles; integration returns this to an output approximately proportional to blood pressure, but mediated by intervening tissue, as discussed below.

3.3. Piezoelectric sensor: mechanical

The piezoelectric sensor responds predominantly to tangential stress or strain in the PVDF ring as it stretches in response to fluctuations in pressure and volume inside the underlying arteries. However, the pressure experienced by the PVDF ring is not identical to the underlying arterial pressure, due to additional tissue dynamics. To approximate this behavior, a very simple mechanical model is used, that also supports dynamic modeling of viscoelastic effects seen to be important to artery and sensor behavior.

The mechanical model used in this work consists of a thick-walled cylinder for the artery including a nonlinear elastic modulus approximation, other soft tissue and skin approximated as a compressible volume, and a linear elastic ring approximation for the sensor, as shown in Fig. 5. A basic assumption of mechanical model is that the artery can be treated as straight and the cross-sectional properties of tissue and bone display minimal changes over the width of PVDF sensors (< 1 cm) compared to overall artery and limb length. The peripheral artery is approximated using a linear thick-walled elastic tube model,

$$\frac{\delta r_i}{\bar{r}_i} = \frac{1}{E(r_i)}\left[f_{ii}(\bar{r}_i, \bar{r}_o)\delta p_i - f_{io}(\bar{r}_i, \bar{r}_o)\delta p_o\right] \tag{6}$$

$$\frac{\delta r_o}{\bar{r}_o} = \frac{1}{E(r_o)}\left[f_{oi}(\bar{r}_i, \bar{r}_o)\delta p_i - f_{oo}(\bar{r}_i, \bar{r}_o)\delta p_o\right] \tag{7}$$

Where $\bar{r}_i$ and $\bar{r}_o$ are the average inner and outer radius of the artery wall, δr_i and δr_i are their variation in time during a cardiac cycle, E is artery elastic modulus, δp_i is pressure change inside the artery, and δp_o is pressure change as experienced by the sensor, which may differ from δp_i due to internal stresses in the artery walls and compressibility of intervening tissue but is assumed to approximately isotropically resist arterial expansion. f_{ii}, f_{oi} f_{io}, and f_{oo} are functions for circumferential stress at the inner (i) or outer (o) radius of the artery. It should be noted that f_{ii}, f_{oi} f_{io}, and f_{oo} are not independent parameters, but are standard functions of $\bar{r}_i$ and $\bar{r}_o$ for a uniform thick-walled elastic tube, as defined in [28].

The piezoelectric sensor response is modeled as thin-walled cylinder subject to approximately uniform pressure from the underlying tissue (p_o) and an initial tension, T, in the sensor. Perturbations of the sensor radius, δR, from its nominal radius, $\bar{R}$ are modeled in the form

$$\delta R = \frac{2\bar{R}^2}{E_s t}\delta p_o - \frac{\bar{R}}{E_s t}\delta T \tag{8}$$

Where E_s is the composite modulus of the PVDF and polyimide layers, t is the sensor band thickness, and δT represents any external perturbations to tension in the sensor, though in this study T is generally held constant.

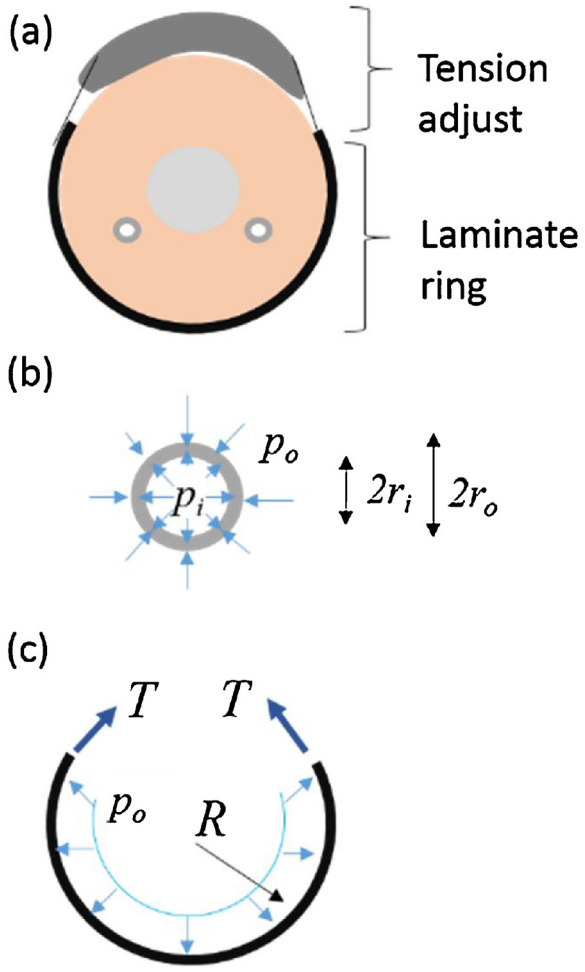

Fig. 5. (a) Schematic drawing of finger cross section with free-body diagrams of (b) artery with internal and external radii r_i and r_2 subject to internal and pressures p_i and p_o (c) and ring sensor with radius R under tension T constraining artery expansion under simplifying assumption of approximately isotropic pressure distribution under ring.

Interior artery expansion can be related to deformation of the sensor by a conservation of area or volume,

$$\pi\left(\bar{R} + \delta R\right)^2 = 2\pi\left(r_o + \delta r_o\right)^2 + V_o - \gamma\delta p_o \tag{9}$$

where V_o is the nominal cross-sectional tissue area enclosed by the sensor, excluding arteries, and γ is a measure of net intervening tissue compressibility. Two major arteries are known to be present under the appendage being monitored.

Combining (6)-(9) and assuming external tension, T, is fixed, a nonlinear function relating sensor pressure perturbations, δp_o to artery perturbations, δr_o, can be obtained:

$$\pi\left(\bar{R} + \frac{2\bar{R}^2}{E_s t}\delta p_o\right)^2 = 2\pi\left(r_o + \delta r_o\right)^2 + V_o - \gamma\delta p_o \tag{10}$$

3.4. Dynamic effects

It is well known that both artery and skin exhibit viscoelastic behavior that leads to hysteretic behavior during phases of increasing versus decreasing pressure during cardiovascular cycles. Experimental comparison of the PVDF sensor response to blood pressure measurements using a finger cuff, in which pressure is

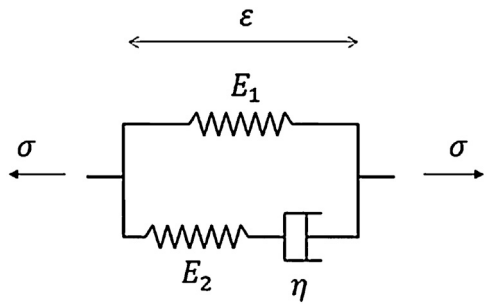

Fig. 6. The Standard Linear Solid Model uses lumped spring and dashpot elements to relate stress, σ, to strain, ε, in a viscoelastic material using two parameters for elastic modulus, E_1 and E_2, and a viscoelasticity parameter, η.

regulated to maintain a constant arterial volume, show a clear hysteresis in piezoelectric signal, consistent with hysteresis arising from viscoelastic effects in tissue. To capture this behavior, a simple viscoelasticity model is added to the mechanical model from Section 3.C. The Standard Linear Solid Model, used here, combines Maxwell model dynamics and a Hookean spring in parallel to relate a stress, σ, to a strain, ε; a viscous material is modeled as a spring and a dashpot in series, both of which are in parallel with a lone spring, as shown in Fig. 6.

For the model in Fig. 6, the governing constitutive relation is:

$$\frac{d\varepsilon(t)}{dt} = \frac{\frac{E_2}{\eta}\left(\frac{\eta}{E_2}\frac{d\sigma(t)}{dt} + \sigma(t) - E_1\varepsilon(t)\right)}{E_1 + E_2} \tag{11}$$

where σ is the applied stress, E_1 and E_2 are elastic moduli describing the tissue, η is a viscoelasticity coefficient, and ε is the strain. Defining $\varepsilon(t) = \delta r_0/\bar{r}_o$ and $\sigma(t) = f_{oi}\delta p_i - f_{oo}\delta p_0$ from the thick wall cylinder model and combining (6), (9), and (11), a constitutive relation between arterial variation and inner and outer pressure under the PVDF ring can be obtained accounting for viscoelasticity,

$$\frac{d\varepsilon}{dt} = \frac{\left(f_{oi}\frac{dp_i}{dt} - f_{oo}\frac{dp_o}{dt}\right) + \frac{E_2}{\eta}\left(f_{oi}\delta p_i - f_{oo}\delta p_o\right) - \frac{E_2}{\eta}E_1\varepsilon}{E_1 + E_2} \tag{12}$$

Changes of inner pressure also be related to other variables by an alternative arrangement of (12), i.e.

$$\frac{dp_i}{dt} = \frac{E_2}{\eta}\frac{\left(f_{oo}\frac{\eta}{E_2}\frac{dp_o}{dt} + f_{oo}\delta p_o - f_{oi}\delta p_i\right) + \left(\frac{\eta(E_1+E_2)}{E_2}\frac{1}{r_o}\frac{dr_o}{dt}\right) + E_1\frac{\delta r_o}{r_o}}{f_{oi}} \tag{13}$$

It should be noted that assignment of viscoelastic effects to the artery alone, computed in terms of r_o is done to simplify model behavior, but effectively lumps in viscoelastic behavior from other sources, such as skin and intervening tissue, when model identification is performed. An alternate approach would be add viscoelastic effects as related to entire limb radius, R, and conceptually should be possible to implement with nearly equivalent results. Practically, placing the primary effect at the artery has been observed to give better matching of hysteresis trends versus measured SVR.

3.5. Model summary

To summarize the sensor model, two independent equations are present: a static relationship relating perturbations in pressure on the sensor to arterial radius (δp_o vs δr_o), in (9) and a dynamic equation for either artery radius or internal pressure (12) or (13) incorporating basic viscoelastic behavior, with variables δp_i, δp_o, and δr_o. Once δp_o can be measured, as with the PVDF sensor, this is sufficient to solve for the other two variables, with δr_i also available via (6) and (7).

However, all the above relationships are dependent on the average arterial radii during the cardiac cycle ($\bar{r}_i$ and $\bar{r}_o$) which in reality will vary over many cycles as vascular resistance changes. Thus, the model is used in inverted fashion for nominal arterial radii, taken to remain constant, as shown schematically in Fig. 7. Then, an input-output relationship between PVDF and PPG measurements can be established for parameter identification and peripheral vascular resistance/SVR estimation. Short term fluctuations in pressure on the PVDF band, inferred from piezoelectric sensor output voltage, are used as an input to the nonlinear state-space models (13) for differential arterial pressure. Pressure is then related to inner and outer arterial radii via (6) and (9), with inner radius used to predict blood volume under PPG sensor, which can be compared to $\hat{u}_{PPG}$ the measured PPG response,

Discrepancies between predicted and measured PPG response are then attributed to changes in arterial radius, as described in the following section.

It should be emphasized that much more detailed arterial tissue modeling has been done in previous works on artery and tissue mechanics. Tissue modeling in this work draws only the most apparent features in observed data, and even then associates behavior such as compressibility and hysteresis only with individual model elements, when in reality the tissue structure under the sensor band is quite heterogeneous. In the following sections, model validation is performed by comparing invasive measurements of SVR to that implied by changes in estimated arterial radius using this model, assuming peripheral vascular resistance and SVR to change effectively proportionally.

4. Parameter identification and tracking metrics

4.1. Model parameters

In the sensor and artery model from Section III, exact parameters related to arterial radius and tissue properties are not directly available unless related solely to the PVDF sensor. Instead, repre-

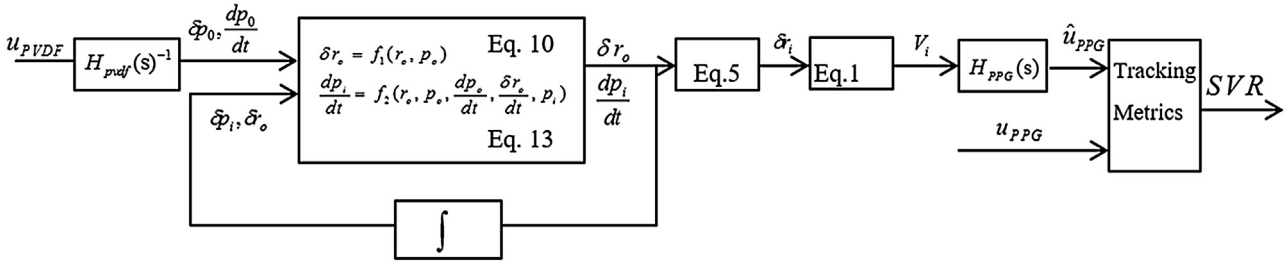

Fig. 7. During implementation, piezoelectric sensor voltage, u_{PVDF}, is used to infer changes in external pressure, p_o, which is used to calculate perturbations in internal artery pressure, p_i, and radii, r_i and r_o via the model from Section 3.4. These estimates are used to predict what changes in internal artery volume, V_i, would be at the nominal artery radius, along with an anticipated PPG sensor output, $\hat{u}_{PPG}$. Comparison to the actual PPG sensor output, u_{PPG} is done to estimate systemic vascular resistance, SVR, by metrics described in Section 4.2.

Table 1
Model Parameters.

Variable	Parameter	Value	Units
Nominal values used throughout testing:			
$\overline{r_o}$	Nominal artery radius	1.5 [31]	mm
$\bar{R}$	limb radius	50	mm
E_s	sensor modulus	2.5 [32]	GPa
t	PVDF thickness	52 [32]	μm
T	ring tension	2	N
d_{31}	piezoelectric coefficient	11×10^{-12} [32]	C/N
γ	ring compliance	1.5	mm^3/Pa
Identified from first 10 cardiac cycles for first swine subject, used in all further testing:			
E_1	viscoelastic modulus 1	200	kPa
E_2	viscoelastic modulus 2	1	kPa
η	viscoelastic damping ratio	1000	
Adjusted for each swine using first 10 cardiac cycles:			
K_{PPG}	PPG gain	2000 ~ 5000	

sentative values from the literature were selected as approximate values, as listed in Table 1. In addition, the gain of the photoplethysmogram was observed to vary substantially from subject to subject, and thus was estimated individually by optimizing the fit between the measured PPG signal and a predicted PPG signal generated from the PVDF sensor measurement at the onset of testing. The first ten cardiac cycles during swine experiments were used to calibrate the PPG gain in each of experiment.

4.2. SVR tracking metrics

As discussed above, neither PPG nor piezoelectric sensing mechanisms provide absolute measurement of arterial radius or pressure, but rather time-varying perturbations from those signals' average values. However, the sensors' relative amplitudes and dynamic responses (i.e., relative hysteresis) remain dependent on artery radius changes. Fig. 8 plots modeled artery volume versus external pressure at the PVDF sensor over a single cardiac cycle for two values of mean arterial radius; experimental measurements for cycles with an approximately equivalent SVR change (as measured invasively) are also shown. First, the model for local tissue and sensor behavior beneath the piezoelectric ring shows acceptable agreement with experimental data, though there is clearly more complexity in the true physiology than in the proposed model.

Second, it is clear that in both the model and experimental behavior, PPG output increases to a proportionally greater degree than PVDF output when mean arterial radius increases and SVR decreases. This provides one method by which changes in arterial radius may be inferred from relative change in PPG and piezoelectric sensor signals.

Third, a key observation during swine testing is that the relative amplitude of hysteresis observed during arterial expansion and contraction correlates very strongly with SVR, which is also observed in Fig. 8: for larger artery radius, the degree of hysteresis changes relative to the total amplitude of the signal.

Based on the observations above, two metrics for estimating changes in peripheral vascular resistance/SVR are proposed. Fig. 9 shows a series of hysteresis loops formed by plotting PPG sensor output versus PVDF sensor output at series of cardiac cycles occurring over a two-hour period. Solid loops indicate experimentally obtained data, with SVR know to be changing and presumed to be accompanied by arterial radius changes. Dashed loops are generated using measured piezoelectric sensor data to predict PPG response if arterial radius were constant, using the model from Section III. Mismatch between the predicted and observed sensor behavior is taken to be indicative of changes in arterial radius.

The metrics proposed SVR tracking using PPG/PVDF information are quantified through linear regression of PPG/PVDF hysteresis

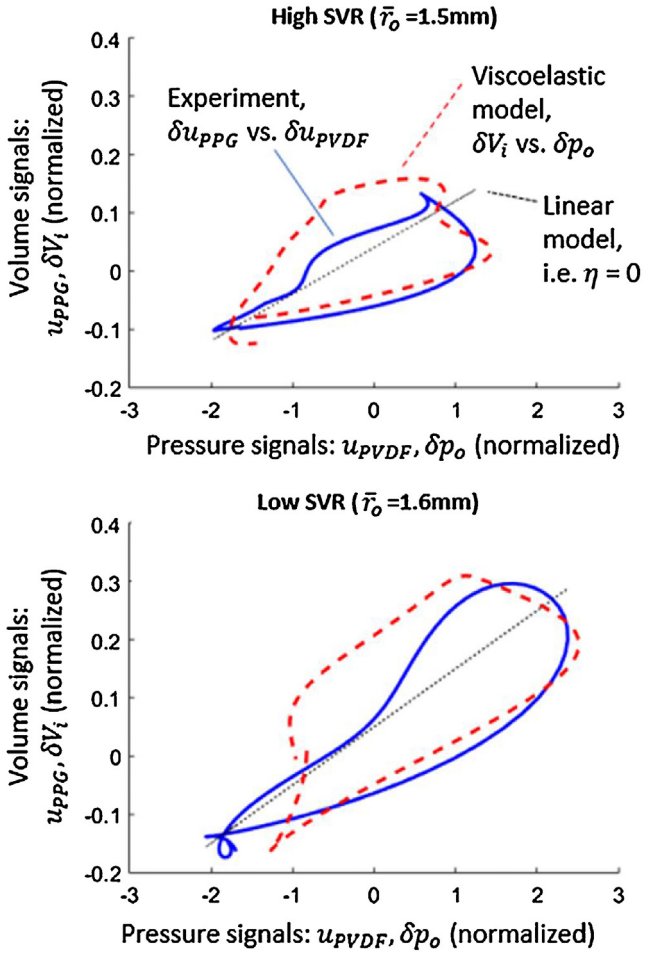

Fig. 8. Hysteretic response is visible between differential pressure and volume during arterial expansion and contraction in both experimental sensor outputs and modeled internal volume vs. external pressure model, but only when using viscoelastic behavior in mechanical model.

loop features of the PPG/PVDF against a small sample (ten cardiac cycles) of invasively measured SVR from an initial swine subject. During each cardiac cycle an ellipse is generated for the best least squares fit of the hysteresis loop between the PPG and piezoelectric sensor outputs for both the experimental and projected (hypothetical fixed radius) response, as shown in Fig. 10. The first feature that was correlated with invasive SVR was the difference in projected and measured amplitude of the signals, measured using the long

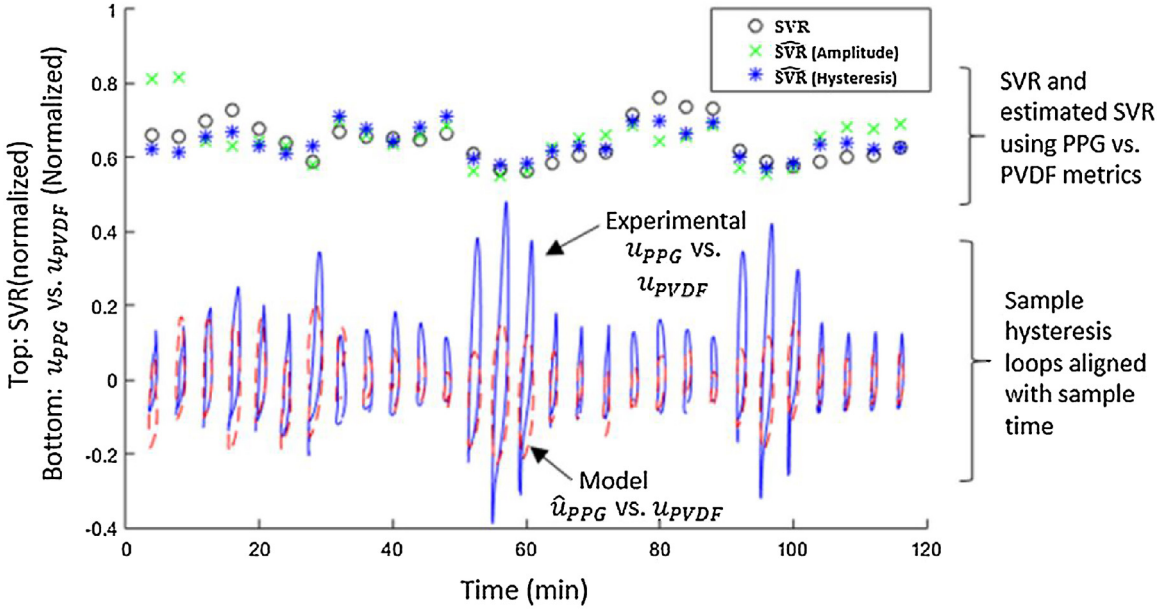

Fig. 9. Examples of hysteresis behavior and SVR tracking over a two-hour experiment, with individual cardiac cycles shown below to demonstrate changes in amplitude and hysteresis behavior, aligned with times at which sample hysteresis loops were collected.

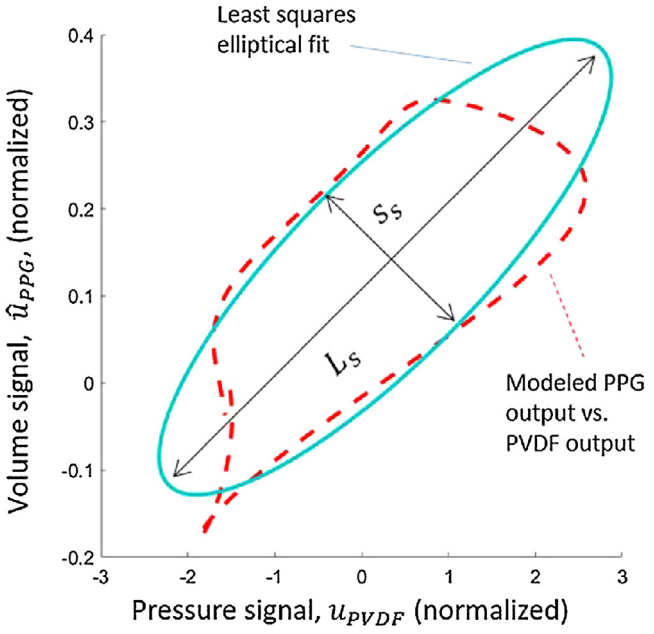

Fig. 10. Sample elliptical fit to modeled PPG vs. measured PVDF output over a sample cardiac cycle, showing hysteresis features used for correlation and estimation of SVR.

chord of the projected ellipse at a fixed model radius, L_s, and the long chord of the experimentally obtained ellipse, L_e. Using these measurements, normalized SVR is estimated as

$$\hat{SVR}_1 = 0.02\,(L_s - L_e) + 0.52 \tag{13}$$

with L being the long chord of an ellipse fit, where subscript s indicates the simulated PPG output given the current PVDF output and subscript e indicates the actual experimental output. Effectively, this metric is selected to capture the mismatch increased signal amplitude when arterial radius changes from baseline, while the ratio of PPG amplitude to PVDF amplitude remains approximately constant if only blood pressure changes at a fixed nominal arterial radius.

Similarly, when SVR increases, observed experimental hysteresis is larger than projected based on the model with constant nominal radius. Again, based on linear regression from the initial cycles of testing with swine 1, this is quantified as

$$\hat{SVR}_2 = -0.166\,(h_s - h_e) + 0.7 \tag{14}$$

where h is a hysteresis measurement obtained from

$$h_{s,e} = \frac{L_{s,e} - S_{s,e}}{L_{s,e}} \tag{15}$$

where S is the short chord of the ellipse fit to the hysteresis loop.

Regression against initial swine subject data is necessary to scale the proportional changes in sensor output to the same proportional change and baseline of SVR. In this work, both metrics are selected to scale measured and estimated SVR to a normalized zero-to-one scale, with one corresponding to the maximum SVR observed. The bias terms in (13) and (14) are also dependent on the PPG gain, which changes from animal to animal and changes the nominal size of the PPG output. This is compensated for through calibration of the PPG gain using only non-invasive data as described in Section 4.1. In most practical applications, baseline SVR would not be known, so the SVR metrics above would provide estimates of relative change in SVR from an initial baseline, not generally absolute SVR. Examples of changes in SVR and metric outputs for a swine subject are shown at the top of Fig. 9 for the sample cardiac cycles shown.

To avoid potential distortion of the hysteresis loops from changes in pulse transit time, the sensors are placed as closely as possible on the swine, approximately 1 cm apart. This corresponds to an estimated time delay of less than 0.1s. In our standard analysis, this time adjustment is applied before providing data to the model by aligning the first PPG and PVDF peak times, but omitting this adjustment to check sensitivity to transit time was found to have negligible effect on the radius and SVR estimates, with the minor change in hysteresis measures (<10%) being proportional between high-SVR and low-SVR scenarios. It has been suggested by past researchers that arterial condition can be related to pulse transit time (PTT) [29,30], and possible correlation of delay between the two sensors and invasive SVR was observed, but this delay in

Table 2
SVR estimation performance for different methods: By hysteresis = estimated based on variation in PPG vs. PVDF hysteresis; By relative amplitude = estimated based on change in relative PPG vs. PVDF amplitude; By PPG wave alone = estimated based on features of PPG waveform.

Test	Mean absolute percentage error			Maximum percentage error			Root mean square error (RMSE)		
	By hyst-eresis	By relative amplitude	By PPG wave alone	By hyst-eresis	By relative amplitude	By PPG wave alone	By hyst-eresis	By relative amplitude	By PPG wave alone
1	4.7%	8.7%	10.2%	14%	29%	50%	0.036	0.072	0.074
2	3.7%	8.0%	9.6%	17%	27%	41%	0.037	0.073	0.093
3	4.5%	5.6%	12.4%	15%	19%	77%	0.037	0.047	0.112

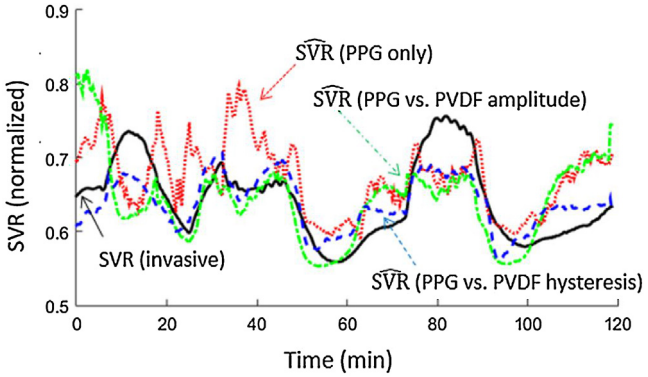

Fig. 11. SVR tracking results for swine test 1.

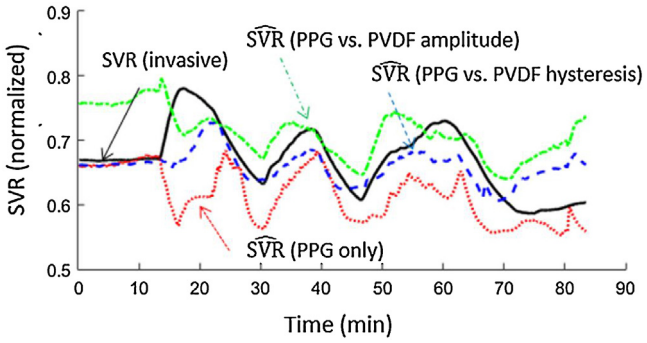

Fig. 12. SVR tracking results for swine test 2.

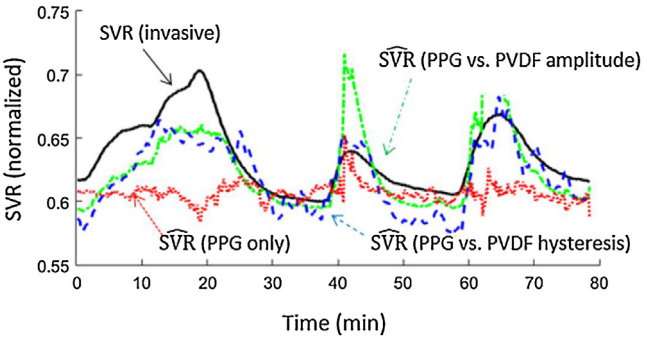

Fig. 13. SVR tracking results for swine test 3.

the current testing arrangement is too short to make use of with sufficient resolution of delay time variation.

5. Results

5.1. Experimental procedure

Proposed metrics for SVR tracking were tested on three swine experimental subjects. SVR was tracked invasively using carotid artery catheterization. SVR was calculated using mean arterial pressure (MAP), central venous pressure (CVP) and cardiac output (CO) using the SVR definition SVR = 80*(MAP-CVP)/CO. Mean arterial pressure was obtained through cannulation of the carotid artery, while CO and CVP were obtained using a Swan Ganz oximetry thermodilution catheter. Data was sampled at 200 Hz, though cardiac output measurements were updated only once per second.

The PVDF sensor and PPG sensor were placed adjacent to one another on same swine appendage (forearm). All the signals were collected and stored using a Biopac MP150 device and analyzed retrospectively. Norepinephrine (a powerful arterial vasoconstrictor agent) was infused into the blood to periodically increase SVR during each test, and SVR dropped when each infusion stopped.

5.2. SVR tracking performance

SVR estimates obtained by the proposed SVR tracking metrics are shown in Figs. 11–13. SVR tracking was most accurate with the first subject, Fig. 11, which showed generally close agreement between both amplitude- and hysteresis-based SVR estimates and invasive SVR measurements after an initial time period required for parameter identification to converge. Greater discrepancies are observed in the second and third tests, but both methods generally capture increases and decreases in SVR. In all three experiments, estimates based on hysteresis variation performed better than estimation based on relative PPG to PVDF amplitude. Worst tracking was observed at the conclusions of experiments with Swine 1 and Swine 2, which may have indicated further physiological changes accumulating during the testing period.

For comparison to existing non-invasive SVR estimation, SVR was also estimated using PPG waveform analysis by the method proposed by A. Scholze et al. [16]. The basic idea of PPG waveform analysis from [16] is that the ratio of first and second peaks of each cardiac cycle is hypothesized to be proportionally related to vascular tone. For data measured from swine subjects, those peaks were identified as the times when the first order derivative of the PPG signal crossed zero, and linear regression to invasive SVR data was applied in the same manner as for the combined PPG/PVDF estimation metrics. SVR estimation based on PPG waveform alone was much less consistent than for metrics combining PPG and piezoelectric sensor information. For example, PPG-only estimates showed good agreement with invasive SVR in test 1, but very poor tracking of SVR in test 3.

Estimator performance was evaluated based various criteria, including root mean square error (RMSE), and mean and maximum absolute percentage errors of SVR tracking, as defined by

$$\frac{1}{N}\sum_{n=1}^{N}\frac{|\hat{SVR}-\overline{SVR}|}{\overline{SVR}} \tag{16}$$

and

$$\max_{n}\frac{|\hat{SVR}-\overline{SVR}|}{\overline{SVR}} \tag{17}$$

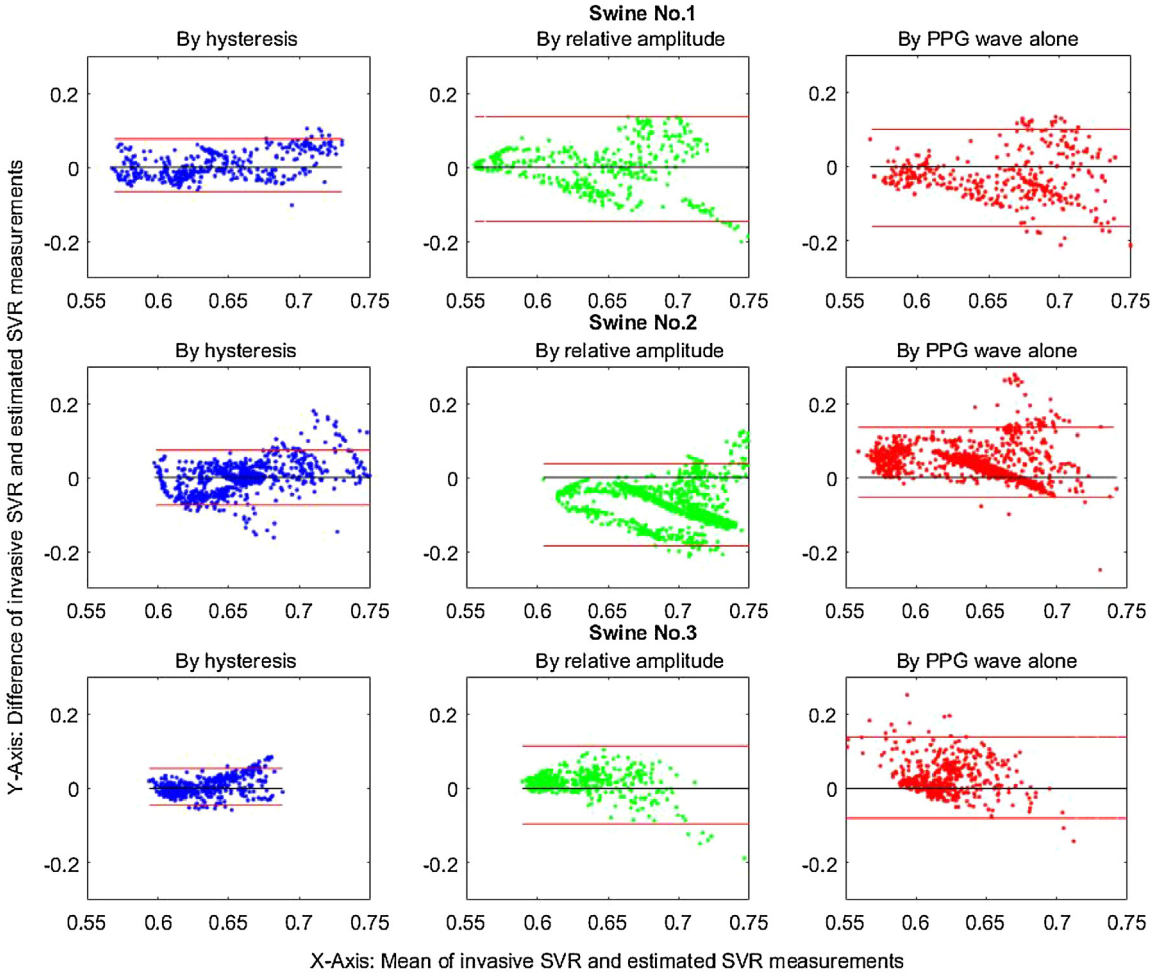

Fig. 14. Bland-Altman plots of SVR tracking results for swine tests.

Table 3
Comparison of estimated and invasive SVR correlation by measures used in prior non-invasive SVR tracking evaluation, for each test and metric applied to PPG and PVDF sensing data. Note that number of subjects and number of samples per subject vary substantially across current and previously reported studies.

			Intraclass correlation (ICC)	R value
BP waveform [17]	Peripheral vascular resistance			0.59
EC [12]	SVR		0.94–0.97	
By hysteresis	SVR	1	0.9735	0.662
		2	0.9933	0.847
		3	0.9583	0.800
By relative amplitude	SVR	1	0.9242	0.466
		2	0.8951	0.683
		3	0.8546	0.740
By PPG waveform	SVR	1	0.8724	0.440
		2	0.8468	0.623
		3	0.4538	0.139

respectively, where N is the number of cardiac cycles and $\overline{SVR}$ is the invasively measurement value for SVR in each cycle.

Performance of non-invasive SVR estimation from combined PPG and piezoelectric sensing, as well as PPG waveform analysis alone is summarized in Table 2. As can be seen, in all three cases the proposed SVR estimator performance was superior to that based on PPG waveform analysis. This was most significant for the worst-case estimates (maximum absolute percentage errors) obtained by each method.

A Bland-Altman plot of estimation results for swine test 2 is shown in Fig. 14. It likewise shows that the estimates based on hysteresis variation performed better than other two methods in both absolute systematic error and proportional error, with PPG/PVDF amplitude-based estimation having a lesser advantage over PPG waveform analysis alone by this view.

5.3. Discussion

The current work proposes a technique for tracking changes in vascular tone by combining information from a photoplethysmogram (PPG) sensor with that from a piezoelectric polymer (PVDF) pressure sensor, worn as a ring or band over peripheral arteries. In a basic sense, the PPG sensor provides a measure of short-term variation in artery volume while the piezoelectric sensor

measures simultaneous surface pressure variations, partially constrained by the sensors mechanical behavior. A simple mechanical model combining a thick-wall cylinder artery model having nonlinear viscoelastic modulus, uniformly compressible soft tissue and a linear elastic piezoelectric sensor ring captures broad features of the relationship between PPG and PVDF signals. Comparing simulated volume changes based on observed surface pressure with the real measurement from the PPG sensor, variations in sensor output attributed to comparatively long-term mean arterial radius variation (and associated increase or decrease in SVR) can be tracked.

We also find that correlation of SVR with estimated SVR by the methods above is comparable to that reported for non-invasive, whole-body measurement technologies as reported in the literature, although the setting in which the methods were applied is very different. This performance is summarized in Table 3. Narula et al. [12] reported an intraclass correlation coefficient (ICC) for SVR based on electrical cardiometry (EC) methods as high as 0.94–0.97 among 50 patients. With combined PPG/PVDF sensing, hysteresis-based intraclass correlation over time for the three swine subjects ranged from 0.95–0.97, while amplitude-based correlation ranged from 0.85–0.92. While the scenarios certainly cannot be considered directly equivalent, due the difference in subjects (humans vs. swine) and testing samples (few samples across many subjects vs. many samples across few subjects), this is suggestive of a potential to eventually estimate SVR with accuracy similar to larger non-invasive clinical systems.

Nonetheless, there remain many limitations to both the modeling and validation methods applied in the current work. First, the proposed tissue model clearly oversimplifies the complex structure of bone, skin, and other soft tissue adjacent to peripheral arteries. This is most clearly seen in the relative additional complexity of experimental vs. modeled hysteresis loops shown in Fig. 8. Prominent omissions from the model include uneven pressure distributions on the sensor, constraints from hard tissue (bone), and longitudinal mechanics of the artery wall extending along the length of the ring. Moreover, the model also isolates viscoelastic behavior in the artery wall, while there are likely to be contributions from most intervening tissue. Nonetheless, the model appears to capture critical changes in sensor behavior as mean arterial radius changes, sufficient to develop SVR tracking metrics as detailed above.

A larger limitation of the current work is the small number of test subjects, though with long monitoring periods available for each. This prevents evaluation of potential complicating factors for estimating SVR as proposed, such as subject age or presence of other cardiovascular disease. In addition, as noted earlier, the non-invasive sensor measurements are more strictly measurements of peripheral vascular resistance, while they are validated against invasive measurements of systematic vascular resistance (SVR). SVR estimation based on sensor measurement effectively assumes that changes in vascular tone are uniform throughout the peripheral vasculature and that this is the dominant factor in changes of SVR for the subject being monitored. However, it remains possible that local peripheral vascular resistance and SVR may diverge under some medical conditions. In addition, without some baseline SVR information, proposed metrics can only provide an estimate of relative changes in SVR from initial application, though this remains important information for patients undergoing critical emergencies such as shock.

6. Conclusion

SVR tracking has been demonstrated on swine subjects using combined information from two non-invasive sensors, a photoplethysmogram (PPG) and a piezoelectric polymer (PVDF) band. SVR tracking is currently performed using simple metrics based on disparate behavior between the sensors when mean artery radius changes. Observed behavior is consistent with a proposed non-linear dynamic model with respect to amplitude and hysteresis of "volume" versus "pressure" trajectories as obtained from the two sensors. Tracking hysteresis showed a very good linear correlation with invasive vascular resistance measurements in swine subjects. The mean absolute error for three experiments were all less than 4.7% using the hysteresis-based strategy, compared 8.7% using the amplitude-based strategy and 12.4% using PPG waveform analysis alone as proposed in prior literature. Performance was also very good by measures used in previous works, albeit in very different testing environments and sampling scenarios.

Future work will involve testing of proposed methods over a larger number of subjects. For example, it remains necessary to verify whether the proposed non-linear viscoelastic dynamic model is feasible with wider tissue variations that are might occur in human subjects. Continuously adaptive methods for tracking changes in radius within the proposed model, or refined versions of the model, will also be tested. If successful, this work may ultimately provide a simple, highly portable method for tracking changes in SVR over time in a variety of medical settings.

Funding

This work was supported by the University of Michigan Center for Integrative Research in Critical Care (MCIRCC), Michigan Translational Research and Commercialization (MTRAC), and the National Science Foundation [grant CMMI-1562254]. K. Najarian, K. Ward, and K. Oldham are members of MCIRCC.

Acknowledgments

The authors thank Mr. Andrew Kuo and Ms. Wenqi Dong for their additional work on piezoelectric sensor hardware and electronics, as well as Dr. Mohamad H. Tiba, Mr. Brendan McCracken and Mr. Gerard Draucker for conducting the animal testing. This work was made possible by the support received from Michigan Center for Integrative Research in Clinical Care (MCIRCC).

References

[1] Y. Magatani, T. Yukioka, S. Ohta, H. Matsuda, H. Shimazu, S. Shimazaki, Vascular tone in patients with hemorrhagic shock, J. Trauma 47 (no. 2) (1999) 282–287.
[2] M. Astiz, E. Tilly, E. Rackow, M. Weil, Peripheral vascular tone in sepsis, Chest 99 (no. 5) (1991) 1072–1075.
[3] J. Siegel, M. Greenspan, L. Del Guercio, Abnormal vascular tone, defective oxygen transport, and myocardial failure in human septic shock, Ann. Surg. 165 (no. 4) (1967) 504–517.
[4] A. Rachev, Remodeling of arteries in response to changes in their mechanical environment, in: Biomechanics of Soft Tissue in Cardiovascular Systems, Springer, 2014, pp. 218–272.
[5] O. Godje, K. Hoke, P. Lamm, C. Schmitz, C. Thiel, M. Weinert, B. Reichert, Continuous, less invasive, hemodynamic monitoring in intensive care after cardiac surgery, Thorac. Cardiovasc. Surg. 46 (no. 4) (1998) 242–249.
[6] B. Straver, M. Roggekamp, P. de Vries, P. de Wee, Systemic vascular resistance in intradialytic hypotension determined by means of impedance cardiography, Blood Purif. 16 (1998) 281–289.
[7] G. Gamble, J. Zorn, G. Sanders, S. MacMahon, N. Sharpe, Estimation of arterial stiffness, compliance, and distensibility from M-mode ultrasound and measurements of the common carotid artery, Stroke 25 (no. 1) (1994) 11–16.
[8] R. Stadler, W. Karl, R. Lees, New methods for arterial diameter measurement from B-mode images, Ultrasound Med. Biol. 22 (no. 1) (1996) 25–34.
[9] A.E. Abbas, F.D. Fortuin, B. Patel, C.A. Moreno, N.B. Schiller, S.J. Lester, Noninvasive measurement of systemic vascular resistance using Doppler echocardiography, J. Am. Soc. Echocardiogr. 17 (no. 8) (2004) 834–838.
[10] N. Fazeli, J.O. Hahn, Estimation of cardiac output and peripheral resistance using square-wave-apaproximated aortic flow signal, Front. Physiol. 3 (2012) 58–67.
[11] J.-J. Wang, J.A. Flewitt, N.G. Shrive, K.H. Parker, J.V. Tyberg, Waves propagating on a windkessel: relation of arterial and venous windkessels to systemic vascular resistance, Am. J. Physiol. 290 (no. 1) (2006) H154–H162.

[12] J. Narula, U. Kiran, S. Chouhan, S. Ramakrishnan, A. Chowdhary, Electrical cardiometry in patients undergoing cardiac cathererisation, Int. J. Perioperative Ultrasound Appl. Technol. 3 (2013) 102–107.
[13] A. Tahvanainen, J. Koskela, M. Leskinen, E. Ilveskoski, K. Norhaussen, M. Kahonen, T. Koobi, J. Mustonen, I. Porsti, Reduced systemic vascular resistance in healthy volunteers with presyncopal symptoms during a nitrate-stimulated tilt-table test, Br. J. Clin. Pharmacol. 71 (no. 1) (2011) 41–51.
[14] V. Sharma, A. Singh, B. Kansara, A. Karlekar, Comparison of transthoracic electrical bioimpedance cardiac output measurement with thermodilution method in post-coronary artery bypasses graft patients, Ann. Card. Anaesth. 14 (no. 2) (2011) 104–110.
[15] R.B. Schnabel, A. Schulz, P.S. Wild, C.R. Sinning, S. Wilde, M. Eleftheriadis, S. Herkenhoff, T. Zeller, E. Lubos, K.J. Lackner, A. Warmnoltz, T. Gori, S. Blankenberg, T. Munzel, Noninvasive vascular function measurement in the community, Circulation: Cardiovasc. Imaging (July) (2011) 371–380.
[16] A. Scholze, A. Burkurt, K. Mardanzai, S. Suvd-Erdene, M. Hausberg, W. Zidek, M. Tepel, Increased arterial vascular tone during the night in patients with esential hypotension, J. Hum. Hypertens. 21 (2007) 60–67.
[17] T. Morise, M. Horita, N. Honda, K. Masuura, I. Kitagawa, R. Shinzato, Y. Hoshiba, H. Masuya, N. Takekoshi, Noninvasive, continuous evaluation of peripheral vascular resistance in humans, Hypertens. Res. 23 (2000) 15–19.
[18] Q.Y. Lee, S.J. Redmond, G.S. Chan, P.M. Middleton, E. Steel, P. Malouf, C. Critoph, G. Flynn, E. O'Lone, N.H. Lovell, Estimation of cardiac output and systemic vascular resistance using a multivariate regression model with features selected from the finger photoplethysmogram and routine cardiovascular measurements, Biomed. Eng. Online 12 (no. 19) (2013) 1–16.
[19] Y.-L. Zheng, B.P. Yan, Y.-T. Zhang, C.C. Poon, Noninvasive characterization of vascular tone by model-based system identification in healthy and heart failure patients, Ann. Biomed. Eng. 10 (2015) 10.1067.
[20] H. Ishihara, M. Tsutui, Impact of changes in systemic vascular resistance on a novel non-invasive continuous cardiac ouput measurement system based on pulse wave transit time: a report of two cases, J. Clin. Monit. Comput. 28 (2014) 423–427.
[21] B. Haslem, A. Gordhandas, C. Ricciardi, T. Heldt, G. Veerghese, Relating noninvasive cardiac output and total peripheral resistance estimates to phsyical activity in an ambulatory setting, Comput. Physiol. 04 (2011) 27–331.
[22] S. Sur, S. Ghatak, An Inexpensive Arterial Pressure Wave Sensor and Its Application in Different Physiological Conditions, arxiv.org, 2005.
[23] Y.-Y. Chiu, W.-Y. Lin, H.-Y. Wang, S.-B. Huan, M.-H. Wu, Development of a piezoelectric polyvinylidene fluoride (PVDF) polymer-based sensor patch for simultaneou heartbeat and respiration monitoring, Sensor Actuat. A: Phys. 189 (2013) 328–334.
[24] C. Dagdeviren, Y. Su, P. Joe, R. Yona, T. Liu, Y.S. Kim, Y. Huang, A.H.J. Damadoran, J. Rogers, Conformable amplified lead zirconate titanate sensors with enhanced piezoelectric response for cutaneous pressure monitoring, Nat. Commun. 5 (2014) 4496, http://dx.doi.org/10.1038/ncomms5496.
[25] S. Gong, W. Schwaib, Y. Wang, Y. Chen, Y. Tang, J. Si, B. Shirnzadeh, W. Cheng, A wearable and highly sensitive pressure sensor with ultrathin gold nanowires, Nat. Commun. 5 (2013) 10.1038.
[26] H.-J. Tseng, W.-C. Tian, W.-J. Wu, Flexible PZT thin film tactile sensor for biomedical monitoring, Sensors 13 (2013) 5478–5492.
[27] J. Allen, Photoplethysmography and its application in clinical physiological measurement, Physiol. Meas. 28 (no. 2) (2007) R1–R39.
[28] J.E. Shigley, C.R. Mischke, R.G. Budynas, Mechanical Engineering Design, McGraw-Hill, 2004.
[29] R. Mukkamala, J.O. Hahn, O.T. Inan, L.K. Mestha, C.S. Kim, H. Toreyin, S. Kyal, Toward ubiquitous blood pressure monitoring via pulse transit time: theory and practice, IEEE Trans. Biomed. Eng. 52 (no. 8) (2015) 1879–1901.
[30] A. Arza, J. Lazaro, E. Gil, P. Laguna, J. Aguilo, R. Bailon, Pulse transit time and pulse width as potential measure for estimating beat-to-beat systolic and diastolic blood pressure, Comput. Cardiol. 40 (2013) 887–890.
[31] V.C. Lopes-Berkas, M.A. Jorgenson, Measurement of peripheral arterial vasculature in domestic Yorkshire swine by using quantitative vascular angiography, J. Am. Assoc. Lab. Anim. Sci. 50 (no. 5) (2011) 628–634.
[32] Precision Acoustics Ltd., PVDF properties and uses, Dorchester, Dorset UK, www.acoustics.co.uk, pp. 1–14, accessed 2016.

Biographies

Lu Wang received the B.E. amd M.E. degrees from Beihang University, Beijing, China, in 2010 and 2013, respectively. He is currently a Ph.D. candidate in the Department of Mechanical Engineering, University of Michigan in Ann Arbor. He is particular interested in sensing, modeling and dynamics, with current research focused on application to the cardiovascular system.

Sardar Ansari is a research fellow at the University of Michigan Department of Emergency Medicine and a member of Michigan Center for Integrative Research in Critical Care (MCIRCC). He earned his Ph.D. in Computer Science and his M.S. degree in Statistics at Virginia Commonwealth University in 2013. Dr. Ansari also received his M.S. degree in Computer Science from VCU in 2010 and his B.S. degree in Software Engineering from University of Tehran, Electrical and Computer Engineering Department in 2008. His research interests are medical signal and image processing, machine learning, data mining and development of medical devices as well as non-linear and discrete optimization and queuing theory

Daniel F. Slavin received B.S. and M.S. degrees in Mechanical Engineering from the University of Michigan in 2014 and 2015, respectively. Interests include dynamic systems and control, with application to various mechatronic systems including biomedical instruments. Mr. Slavin is currently at General Motors, Inc.

Kevin R. Ward is Professor of Emergency Medicine at the University of Michigan. He received his MD from Tulane University School of Medicine in 1989 and post-graduate training in Emergency Medicine from the University of Pittsburgh and the Ohio State University Schools of Medicine. Dr. Ward's research interests lie in the development of scalable diagnostic, device, and digital health platforms in critical care for monitoring and clinical decision making. He serves as the Executive Director of the Michigan Center for Integrative Research in Critical Care designed to bring multidisciplinary team science solutions to the critically ill and injured. He also serves as the Executive Director for the University of Michigan Medical School's Fast Forward Medical Innovation (FFMI) program. FFMI is one of the country's first integrated innovation programs designed to strategically move the University's biomedical ideas to patient impact.

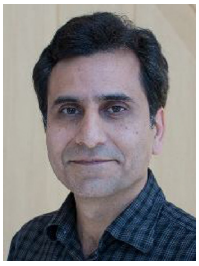

Kayvan Najarian is an Associate Professor in the departments of Computational Medicine and Bioinformatics, and Emergency Medicine at the University of Michigan. He also serves as the director of the Michigan Center for Integrative Research in Critical Care's Biosignal-Image and Computational (BIC) Core program. Dr. Najarian received his Ph.D. in Electrical and Computer Engineering from University of British Columbia, Canada, M.Sc in Biomedical Engineering from Amirkabir University, Iran, and B.Sc. in Electrical Engineering from Sharif University, Iran. The focus of Dr. Kayvan Najarian's research is on the design of signal/image processing and machine learning methods to create computerassisted clinical decision support systems that improve patient care. Dr. Najarian serves as the Editor-in-Chief of a journal in the field of Biomedical Engineering as well as the Associate Editor of two journals in the field of biomedical informatics. He is also a member of many editorial boards and has served as a guest editor of special issues for several journals.

Kenn R. Oldham is an Associate Professor of Mechanical Engineering at the University of Michigan and a member of the Michigan Center for Integrative Research in Critical Care. Prof. Oldham received the Ph.D. in Mechanical Engineering from the University of California at Berkeley in 2006 and the B.S. in Mechanical Engineering from Carnegie Mellon University in 2000. His research focuses on the intersection of dynamics and control with small-scale sensing and actuation. Research interests include design for controllability, system estimation and identification, and novel sensor and actuator design. Applications include terrestrial micro-robotics, endoscopic microscopy, and inertial and physiological sensing.